frontiers in Chemistry

ORIGINAL RESEARCH
published: 14 June 2019
doi: 10.3389/fchem.2019.00437

# Facile Controlled Synthesis of Spinel $LiMn_2O_4$ Porous Microspheres as Cathode Material for Lithium Ion Batteries

*Yun Hai[1], Ziwei Zhang[1], Hao Liu[2]*, Libing Liao[1]*, Peng Fan[1], Yuanyuan Wu[2], Guocheng Lv[1] and Lefu Mei[1]*

[1] Beijing Key Laboratory of Materials Utilization of Nonmetallic Minerals and Solid Wastes, School of Materials Science and Technology, China University of Geosciences, Beijing, China, [2] School of Science, China University of Geosciences, Beijing, China

Although the electrochemical properties of porous $LiMn_2O_4$ microspheres are usually improved compared to those of irregular $LiMn_2O_4$ particles, the effects of the different synthesis conditions on the preparation of the porous $LiMn_2O_4$ microspheres are rarely discussed in detail. In the present work, porous $LiMn_2O_4$ microspheres were successfully synthesized by using molten LiOH and porous $Mn_2O_3$ spheres as a template. Multiple factors were considered in the preparation process, including reagent concentration, pH, adding mode, heating time, etc. The morphology of the $MnCO_3$ template was crucial for the preparation of porous $LiMn_2O_4$ microspheres and it was mainly affected by the concentration of reactants and the pH value of the solution during the precipitation process. During the lithiation of $Mn_2O_3$ microspheres, the heating temperature and the ratio between $Mn_2O_3$ and lithium salt were the most significant variables in terms of control over the morphology and purity of the $LiMn_2O_4$ microspheres. Furthermore, we demonstrated that the porous $LiMn_2O_4$ microspheres presented better rate capability and cyclability compared to commercial $LiMn_2O_4$ powder as cathode materials for lithium-ion batteries (LIBs). This study not only highlights the shape-controllable synthesis of $LiMn_2O_4$ microspheres as promising cathode materials, but also provides some useful guidance for the synthesis of porous $LiMn_2O_4$ microspheres and other LIB' electrode materials.

**Keywords: lithium manganese oxide, microsphere, cathode, lithium ion battery, percipitation, calcination**

OPEN ACCESS

***Edited by:***
*Juchen Guo,*
*University of California, Riverside,*
*United States*

***Reviewed by:***
*Liang Shi,*
*University of Science and Technology of China, China*
*Jingbing Liu,*
*Beijing University of Technology, China*

***Correspondence:***
*Hao Liu*
*liuhao1398@cugb.edu.cn*
*Libing Liao*
*lbliao@cugb.edu.cn*

***Specialty section:***
*This article was submitted to Electrochemistry, a section of the journal Frontiers in Chemistry*

***Received:*** *30 April 2019*
***Accepted:*** *28 May 2019*
***Published:*** *14 June 2019*

***Citation:***
*Hai Y, Zhang Z, Liu H, Liao L, Fan P, Wu Y, Lv G and Mei L (2019) Facile Controlled Synthesis of Spinel $LiMn_2O_4$ Porous Microspheres as Cathode Material for Lithium Ion Batteries. Front. Chem. 7:437. doi: 10.3389/fchem.2019.00437*

## INTRODUCTION

With the development of science and technology, lithium-ion batteries (LIBs) have been widely used in various portable energy storage devices (Wakihara, 2001; Etacheri et al., 2011; Chen D. et al., 2018; Chen H. et al., 2018) such as tablets, smartphones, cameras, etc. Further applications in electric vehicles, hybrid vehicles, military, and aerospace have also been developed and explored (Smart et al., 2004; Park et al., 2010; Lu et al., 2013; Lipu et al., 2018). Among various cathode materials for LIBs, $LiMn_2O_4$ cathode material with a spinel structure—which is cheap, safe and rich in resources—has become a research hotspot (Lee et al., 2010; Qu et al., 2011; Lai et al., 2016; Zhu et al., 2016; Wang et al., 2018).

In long-term charging and discharging, the dissolution of Mn into electrolytes causes capacity degradation and poor cycle performance of cathode materials, which severely restricts the commercial application of $LiMn_2O_4$. Various methods have been tried to improve the electrochemical performance of spinel $LiMn_2O_4$ cathode materials, including surface coating, bulk doping, and morphology control (Iqbal et al., 2012; Tang et al., 2013; Jeong et al., 2015; Xu et al., 2018). Among these improvements, down-sizing of $LiMn_2O_4$ particles can significantly shorten the transport distance of lithium ions in solid, thus helping to improve their rate performance. Therefore, nanostructured $LiMn_2O_4$ with various morphologies has been extensively prepared in recent years (Lee et al., 2010; Tang et al., 2012, 2013). Tang et al. (2012) synthesized a nanochain of $LiMn_2O_4$ by a sol-gel method with a very good rate capability. The result showed a reversible capacity of 100 $mAhg^{-1}$ at rate of about 1 C and 58 mAh $g^{-1}$ at rate of 20 C. Lee et al. (2010) synthesized ultrathin $LiMn_2O_4$ nanowires with diameters <10 nm and lengths of several micrometers, which displayed 100 and 78 mAh $g^{-1}$ at very high rates of 60 and 150 C. Nevertheless, the tap density of the above nanostructured $LiMn_2O_4$ is generally low due to its irregular shape, high surface area, and high porosity (Guo et al., 2014), resulting in low volumetric energy density of the LIBs' electrodes. In contrast, the LIBs' electrodes made of sub-micron-sized spherical active materials usually show higher volumetric energy density (Aurbach et al., 1999; Levi et al., 1999; He et al., 2006), which is caused by the compact packing of spherical particles. Additionally, an ideal structure would be a porous microsphere which consists of nanocrystallites tightly compacted with three-dimensional channels for ion diffusion in consideration of electron transportation distance (Qian et al., 2010; Ren et al., 2014; Yin et al., 2019). This structured $LiMn_2O_4$ can have both high volumetric energy density and high rate capability simultaneously. For example, Liu et al. (2018) reported the synthesis of the porous $LiMn_2O_4$ micro-/nano-hollow spheres from the globe precursor $MnCO_3$ via a facile precipitation route. The obtained $LiMn_2O_4$ delivered excellent cycle stability and almost no capacity loss after 200 cycles. Wang et al. (2013) synthesized porous $LiMn_2O_4$ spheres with pores at an average size of 45 nm. The discharge capacity of the porous sphere $LiMn_2O_4$ was 83 mAh $g^{-1}$ at a rate of 20 C, which showed stable high-rate capability. Although the previous work has reported the preparation of porous $LiMn_2O_4$ microspheres and improvement of their electrochemical properties, the effects of the different synthesis conditions on the $LiMn_2O_4$ morphology and size have been rarely discussed in detail.

Herein, we reported the synthesis of spinel $LiMn_2O_4$ porous microspheres by lithiation of porous $Mn_2O_3$ microspheres. The effects of a series of preparation conditions, including reagent concentration, pH, adding mode, heating time, etc., on the morphology of the $LiMn_2O_4$ microspheres were investigated in detail. Moreover, we compared the electrochemical performance of synthesized $LiMn_2O_4$ microspheres with that of commercial $LiMn_2O_4$ powder. Significantly, without cation doping or surface coating, the porous $LiMn_2O_4$ microspheres present better rate capability and cyclability.

# EXPERIMENTAL

## Materials Synthesis

### Preparation of $MnCO_3$ Microsphere

$LiOH{\cdot}H_2O$ (99.0%, AR) and ethanol (99.7%, AR) were purchased from Aladdin. $MnSO_4{\cdot}H_2O$ (99.0%, AR), $NH_4HCO_3$ (21.0%, AR), $NH_3{\cdot}H_2O$ (25%, AR), and $H_2SO_4$ (98.0 wt.%) were supplied by XiLong Chemical Co. Ltd. All reagents were used without further purification. The spherical $MnCO_3$ was first prepared by a general chemical precipitation method. In a typical synthesis, 0.3042 g $MnSO_4{\cdot}H_2O$ and 1.4231 g $NH_4HCO_3$ were dissolved in 45 mL deionized water and 5 mL ethanol, respectively, to form a transparent solution. After the complete dispersion of the $MnSO_4$ and $NH_4HCO_3$ solutions, the $NH_4HCO_3$ solution was added to the $MnSO_4$ solution rapidly with vigorous stirring. A certain amount of $NH_3{\cdot}H_2O$ (10.0% v/v.) or $H_2SO_4$ (10.0% v/v.) was then added dropwise to adjust the pH value of the suspension to 7.5. The milky white suspension was stirred for 3 h at room temperature and maintained for 5 h. The powder was obtained by filtrating, washing, and drying in the air at 80°C for 24 h to obtain spherical $MnCO_3$ precursors.

### Preparation of $Mn_2O_3$ and $LiMn_2O_4$

The as-obtained $MnCO_3$ powders were heated in air at 700°C for 10 h at a heating rate of $10°C{\cdot}min^{-1}$ to synthesize porous $Mn_2O_3$ spheres. The porous $Mn_2O_3$ spheres were grounded thoroughly with $LiOH{\cdot}H_2O$ in a molar ratio of $Mn_2O_3$:LiOH = 1:1.1 using ethanol as a dispersal agent. Finally, the mixtures were calcined at 650°C for 10 h with a heating rate of $5°C{\cdot}min^{-1}$ in the air to achieve porous $LiMn_2O_4$ spheres.

## Characterization

X-ray diffraction (XRD) characterization was conducted to identify the crystal structure of the samples on an X-ray powder diffractometer (D8 Advance, Bruker, Germany) with a Cu Kα ($\lambda = 0.15406$ Å) radiation. The micro-morphologies of $MnCO_3$, $Mn_2O_3$, and $LiMn_2O_4$ were observed using scanning electron microscopy (FESEM, MERLIN VP Compact, ZEISS, Germany).

## Electrochemical Measurements

The electrochemical performance was evaluated using CR2032 coin cells assembled in a high-purity argon-filled glove box with the moisture and oxygen content maintained below 0.1 ppm. The working electrode consisted of 70 wt.% $LiMn_2O_4$ spheres, 20 wt.% acetylene black and 10 wt.% polyvinylidene fluoride (PVDF) as a binder. Pure lithium foil was used as the counter electrode. The separator was Celgard 2400. The electrolyte was 1.0 M $LiPF_6$ in ethylene carbonate/ethyl methyl carbonate/dimethyl carbonate solvent (1:1:1 v/v/v, Shenzhen Keijing Star Tech. Co.). The cells were aged for 12 h before measurement. All cyclic voltammogram tests were performed on an electrochemical workstation (Ivium-Vertex, Ivium Technologies, Holland). The galvanostatic charge/discharge tests were carried out using a Battery Testing system (CT-4008, NEWARE, China) with a voltage window of 3.0–4.5 V vs. $Li^+$/Li at room temperature.

# RESULTS AND DISCUSSION

## The Synthesis Principle and Process of $LiMn_2O_4$ Microspheres

**Figure 1** shows the schematic of the preparation of the spinel $LiMn_2O_4$ porous microspheres. First, $MnCO_3$ microspheres as precursors are synthesized based on a precipitation method through the reaction of the $MnSO_4$ solution with the $NH_4HCO_3$ solution. Secondly, $MnCO_3$ microspheres are subsequently transformed into $Mn_2O_3$ microspheres through the decomposition by heating treatment in tube furnace. Finally, $LiMn_2O_4$ microspheres are obtained by the lithiation reaction of $Mn_2O_3$ porous microspheres with LiOH at high temperature. The influences of the key parameters in each of the above processes on the microstructures and crystallinities of the products are further discussed in detail.

## The Effects of Main Preparation Conditions on the Morphology of $MnCO_3$

The first step is to synthesize $MnCO_3$ microspheres successfully, which is a key for the preparation of $LiMn_2O_4$ microspheres. We have successfully prepared the $MnCO_3$ microspheres using precipitation. Powder X-ray diffraction analysis of spherical products after the precipitation reaction was employed to identify the crystallographic phase. **Figure 2a** shows the XRD pattern of the obtained products and the standard pattern of $MnCO_3$. All the diffraction peaks can be indexed to the well-crystallized hexagonal $MnCO_3$ (JCPDS#44-1472). No other impurities can be observed in the XRD pattern. **Figures 2b,c** displays the SEM images of spherical $MnCO_3$. It is evident that $MnCO_3$ spheres are uniform and monodispersed with rough surface with an average diameter of about 1.0 μm. In addition, we found that the morphology of the $MnCO_3$ was greatly influenced by the preparation conditions during the precipitation. Therefore, we have studied the effects of the main preparation conditions in the precipitation process of the synthesis of $MnCO_3$.

### The Effects of $MnSO_4$ Concentration on the Morphology of $MnCO_3$

The SEM images of $MnCO_3$ prepared at the different concentrations of the $MnSO_4$ solution are shown in **Figure 3**. During the preparation, the concentration of $NH_4HCO_3$ was 0.36 M, and other synthesis conditions were maintained. When the concentration of $MnSO_4$ solution is 0.02 M, the morphology of $MnCO_3$ tends to form more cubes than spheres (**Figure 3a**). With the increase of the $MnSO_4$ concentration to 0.036 M, their morphology gradually transforms from cubical to spherical shapes (**Figure 3b**). When the concentration of the $MnSO_4$ solution is higher than 0.10 M, the morphology of $MnCO_3$ becomes an irregular granular shape (**Figures 3c,d**).

### The Effects of $NH_4HCO_3$ Concentration on the Morphology of $MnCO_3$

**Figure 4** shows the SEM images of $MnCO_3$ prepared at different concentrations of the $NH_4HCO_3$ solution. During the preparation, the concentration of the $MnCO_3$ solution was 0.036 M, and the other synthesis conditions were maintained. When the $NH_4HCO_3$ concentration is 0.09 M, the morphology of $MnCO_3$ is irregular. With the increase of the $NH_4HCO_3$ concentration to 0.18 M, the morphology of $MnCO_3$ tends to form spheres. When the concentration of $NH_4HCO_3$ is 0.36 M, the $MnCO_3$ spheres own uniform size and good dispersion. The particle size varies from 0.5 to 1.8 μm, mainly in the range of 1.1–1.4 μm, and the average particle size is about 1.0 μm. When the concentration of $NH_4HCO_3$ goes higher as 0.54 M, the spherical $MnCO_3$ becomes larger and has a clear agglomeration.

### The Effects of Solution pH on the Morphology of $MnCO_3$

Solution pH proved to be a crucial factor in the controlled formation of the final products (Hong et al., 2003; Kloprogge et al., 2004; Kong et al., 2019; Simon et al., 2019). Herein, the synthesis process in different pH of the above solution was investigated. **Figure 5** shows the SEM images of $MnCO_3$ prepared at different pH. When the pH is 6.5 and 7.0, $MnCO_3$ displays morphologies that are a mixture of cubes and irregular shapes (**Figures 5a,b**). With the increase of pH value to 7.5, the spherical morphology forms (**Figure 5c**). When the pH value reaches to 8.0, the size of the microspheres becomes uneven and seriously agglomerated (**Figure 5d**). This can be explained by the relationship between the pH of the solution and the hydrolysis process of the reactants. An increase in pH can lead to an increase in the hydrolysis rate (Nagao et al., 2004; Hussain et al., 2017). In the reaction process, when the pH value is higher, the hydrolysis of $NH_4HCO_3$ and $MnSO_4$ are more complete, which accelerates the formation of $MnCO_3$ microspheres, but a hydrolysis speed that is too fast is not conducive to controlling the properties of particles, which will widen the particle size distribution. Instead, the low pH will cause incomplete hydrolysis and irregular appearance of final products.

### The Effects of Addition Mode on the Morphology of $MnCO_3$

In addition to the effect of reagent ratio and pH, the addition mode of $NH_4HCO_3$ also has a significant impact on the size and morphology of the synthesized samples. Two synthetic methods—adding the $NH_4HCO_3$ dropwise and pouring it directly into the $MnSO_4$ solution—were employed in our experiment. The SEM results of corresponding products are displayed in **Figure 6**. As shown in **Figure 6a**, drop-by-drop addition of $NH_4HCO_3$ solution into the $MnSO_4$ solution leads to large differences in the size of the $MnCO_3$ microspheres, with the average size being 1.95 μm. On the contrary, the size of the $MnCO_3$ microspheres is more uniform and the average size reduces to 0.99 μm (**Figure 6b**) in the later method. This is probably because the nucleation of $MnCO_3$ was continuously formed in the solution during the drop-by-drop addition of $NH_4HCO_3$, leading the small microspheres that were formed to be accompanied by the growth of existing microspheres in the solution. In contrast, when the $NH_4HCO_3$

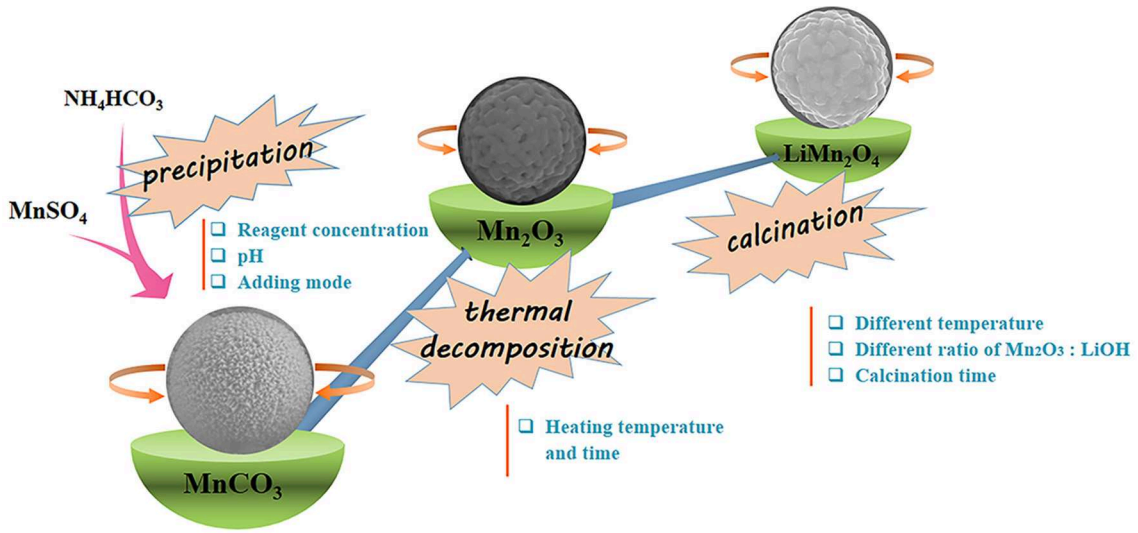


**FIGURE 1 |** Schematic of the preparation of the spinel $LiMn_2O_4$ porous microspheres.

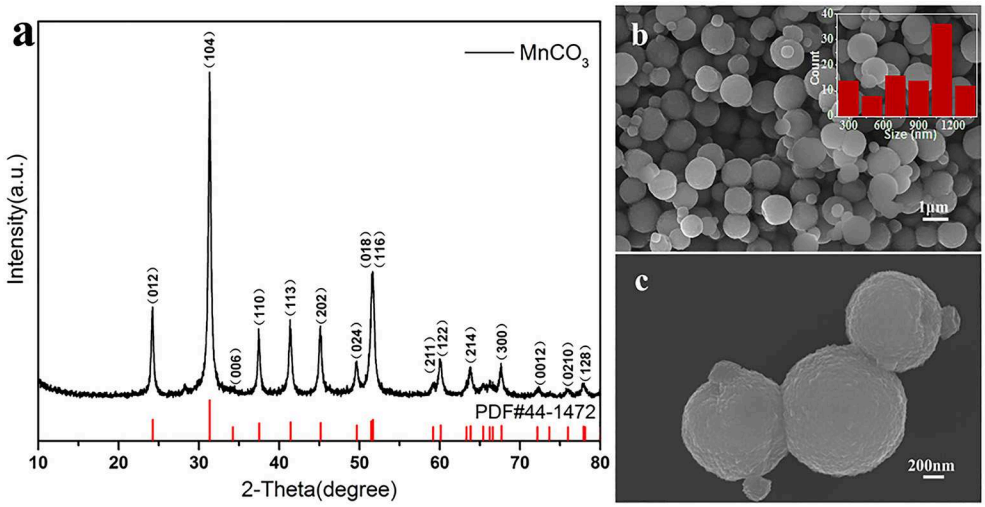


**FIGURE 2 | (a)** XRD pattern of $MnCO_3$ and the standard pattern of $MnCO_3$ (PDF#44-1472) is shown as reference; **(b,c)** SEM images of $MnCO_3$ at different magnification. The inset shows the size distribution of these particles.

solution was directly poured into the $MnSO_4$ solution, the nucleation of $MnCO_3$ was formed in a short time and grew up simultaneously. Therefore, the size of the $MnCO_3$ microspheres is more uniform.

## The Effects of Heating Temperature and Time on the Morphology of $Mn_2O_3$

The second step is to synthesize $Mn_2O_3$ porous microspheres through the decomposition of the $MnCO_3$ microspheres by heating treatment. The porous structure of $Mn_2O_3$ microspheres is important for the synthesis of $LiMn_2O_4$ microspheres without structural collapse because this structure can provide more grain shrinkage space during the lithiation process of $Mn_2O_3$ microspheres. We have investigated the influences of the heating temperature and heating time on the morphology of $Mn_2O_3$. The XRD result and SEM images of the corresponding samples are shown in **Figure 7**. During the decomposition process, the solid phase changes from $MnCO_3$ to $Mn_2O_3$ with the release of $CO_2$. Reversible oxidation and formation of various manganese oxides occur in the range of 350–560°C (Biernacki and Pokrzywnicki, 1999; Wang et al., 2013), and ultimately, pure phase of $Mn_2O_3$ is formed at above 600°C. **Figure 7a** shows the XRD pattern of $Mn_2O_3$ heated at 600°C for 5 h. All the peaks are identical to the pure phase of $Mn_2O_3$ (JCPDS#71-0636), which is consistent with the phase transition process in the literature (Wang et al., 2013). On the other hand, a porous microsphere structure consisting

of small $Mn_2O_3$ nanocrystals are formed after heating for 5 h (**Figure 7b**). Furthermore, the EDS result (**Figure 7c**) also proves that $MnCO_3$ has been fully reacted. When the heating time is increased to 10 and 20 h, the spherical shape of the $Mn_2O_3$ porous microspheres is well-maintained, but the sizes of the nanocrystallites increase slightly (**Figures 7d,e**). As the heating temperature increases to 700°C for 10 h, the nanocrystallites of the $Mn_2O_3$ porous microspheres increase obviously in size and partial microspheres show large holes in the surface (**Figure 7f**). The above results indicate that both extension of heating time and increase of heating temperature leads the $Mn_2O_3$ crystallites to grow into larger ones by adsorbing surrounding primary particles.

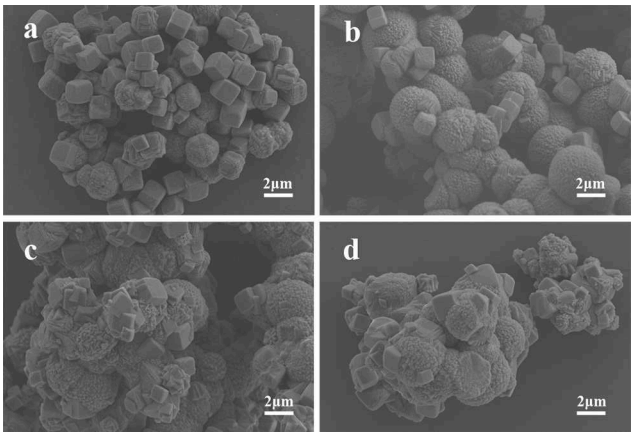


**FIGURE 3 |** SEM images of $MnCO_3$ prepared at different concentrations of $MnSO_4$ solution. **(a)** 0.02 M; **(b)** 0.036 M; **(c)** 0.10 M; **(d)** 0.20 M.

## The Effects of Calcination Temperature, Calcination Time, and $Mn_2O_3$:LiOH Molar Ratio on the Synthesis of $LiMn_2O_4$

The last step for the synthesis of the $LiMn_2O_4$ spheres is the lithiation reaction of $Mn_2O_3$ porous microspheres with LiOH at high temperature. There are influences of the calcination temperature, calcination time and $Mn_2O_3$:LiOH molar ratio on the synthesis of $LiMn_2O_4$ microspheres. At first, the calcination temperature was adjusted in the range of 600–750°C, and the calcination time and molar ratio of $Mn_2O_3$:LiOH were set as 5 h and 1:1.05, respectively. **Figure 8** shows the XRD patterns and SEM images of the corresponding samples. In **Figure 8a1**, for all the samples, the main characteristic peaks can be indexed as spinel $LiMn_2O_4$ (JCPDS#35-0782), but there is also a small weak peak at 32.9° originating from unreacted $Mn_2O_3$, indicating a slight deficiency in the amount of lithium. It is apparent in **Figures 8a3,a4** that the porous spherical structure is well-preserved. It is also clear that $LiMn_2O_4$ spheres are composed of aggregated nanocrystallites with pores existing among them. Compared with the samples heated at 650 and 700°C, a small fraction of broken spheres can be observed in the products under 600°C (**Figure 8a2**). In **Figure 8a5**, the samples are piled up by irregular particles, and the holes disappeared. This is due to the structural collapse caused by excessive sintering temperature.

Next, we attempted to increase the molar ratio of $Mn_2O_3$:LiOH to 1.10 and 1.50 to obtain pure spinel $LiMn_2O_4$.

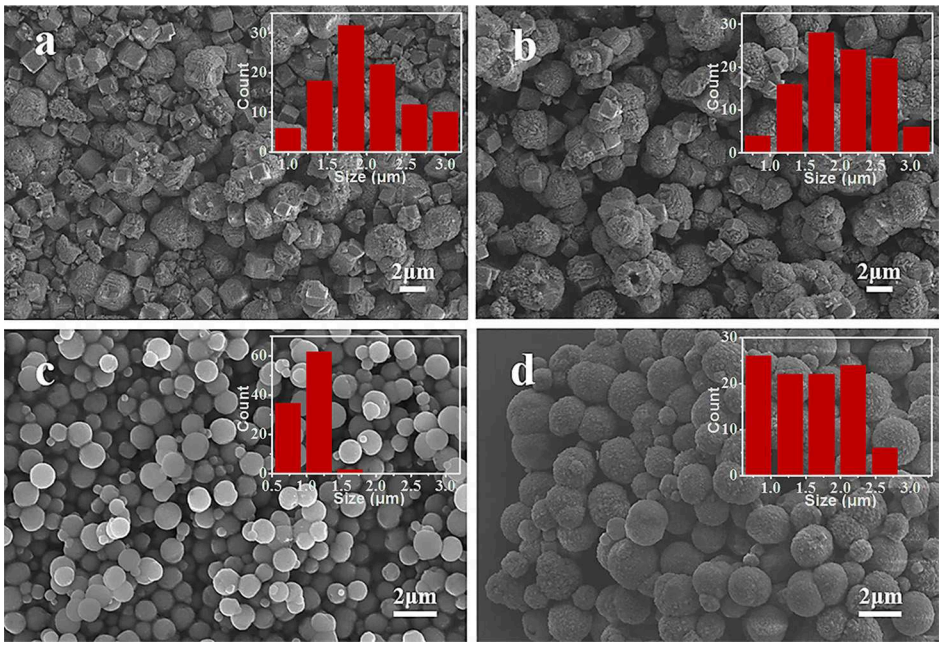


**FIGURE 4 |** SEM images of $MnCO_3$ prepared at different concentrations of $NH_4HCO_3$ solution. **(a)** 0.09 M; **(b)** 0.18 M; **(c)** 0.36 M; **(d)** 0.54 M. The inset shows the size distribution of these particles.

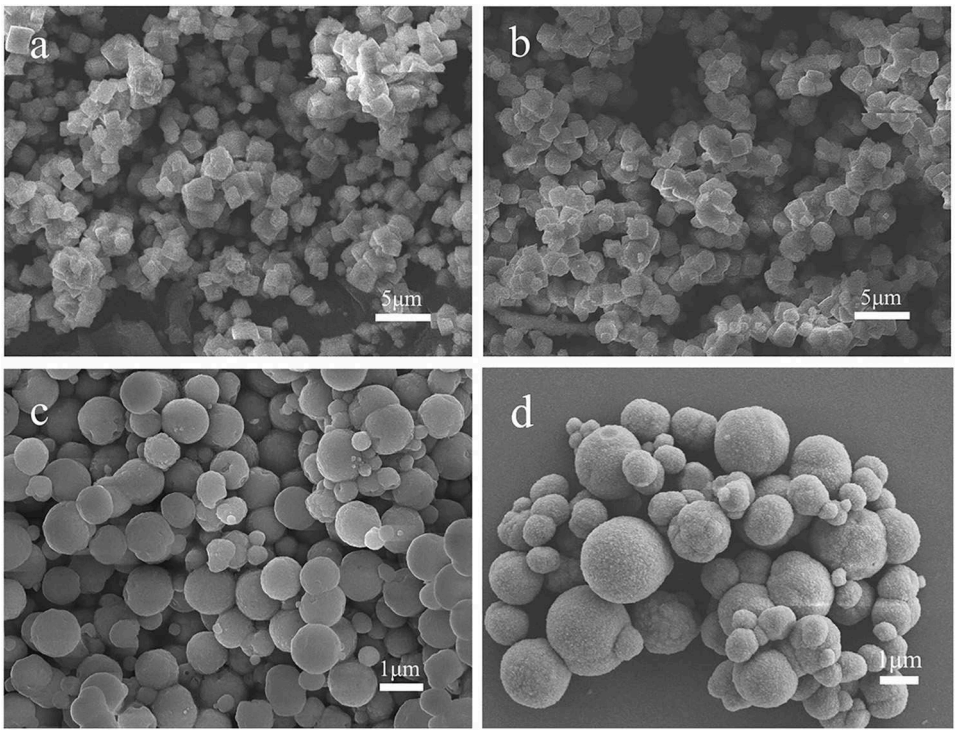


**FIGURE 5 |** SEM images of $MnCO_3$ prepared at different solution pH of 6.5 **(a)**, 7.0 **(b)**, 7.5 **(c),** and 8.0 **(d)**.

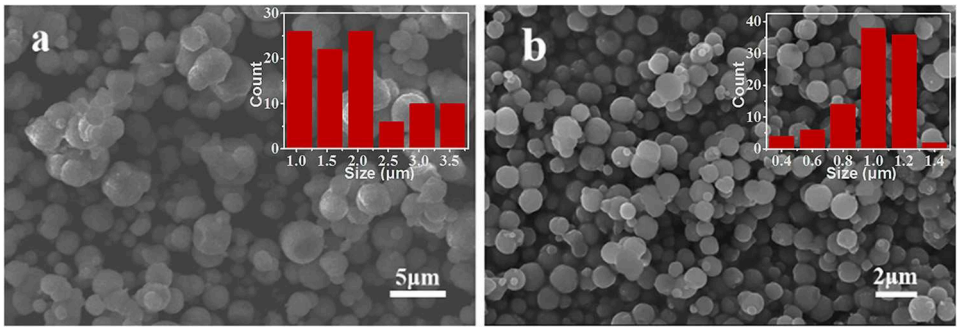


**FIGURE 6 |** SEM images of $MnCO_3$ prepared at different adding mode of $NH_4HCO_3$ solution. **(a)** Added dropwise, **(b)** poured directly. The inset shows the size distribution of these particles.

**Figure 8b1** shows the XRD patterns of the samples synthesized at 650°C with different time. When the molar ratio of $Mn_2O_3$:LiOH reaches 1:1.1 and the calcination time is 5 h, the lithiation reaction is incomplete, remaining as unreacted $Mn_2O_3$. With the extension of calcination time to 10 h, all the diffraction characteristic peaks in the XRD patterns can be identified with standard $LiMn_2O_4$ (JCPDS#35-0782), indicating good crystallinity and high purity for the products. Nevertheless, when the molar ratio of $Mn_2O_3$:LiOH further increases to 1.50, a new characteristic peak appears at 44.8°, which is indexed as $Li_2MnO_3$ (JCPDS#27-1252) phase, indicating that the lithium is excessive in this molar ratio. The above results suggest that the synthesis of pure $LiMn_2O_4$ requires an appropriate range for the molar ratio of $Mn_2O_3$:LiOH, and it is easy to produce byproducts beyond or under the critical values. The morphology and particle size of the products are observed by SEM. As can be seen from **Figure 8b2** through **Figure 8b5**, $LiMn_2O_4$ is composed of uniform microspheres with a rough surface. The diameter of the microspheres is in the range of 0.8–1.0 μm.

## Electrochemical Properties of $LiMn_2O_4$ Microspheres

The electrochemical performance of synthetic porous $LiMn_2O_4$ spheres was discussed as a cathode material for a lithium-ion battery. The cyclic voltammogram (CV) of the synthesized

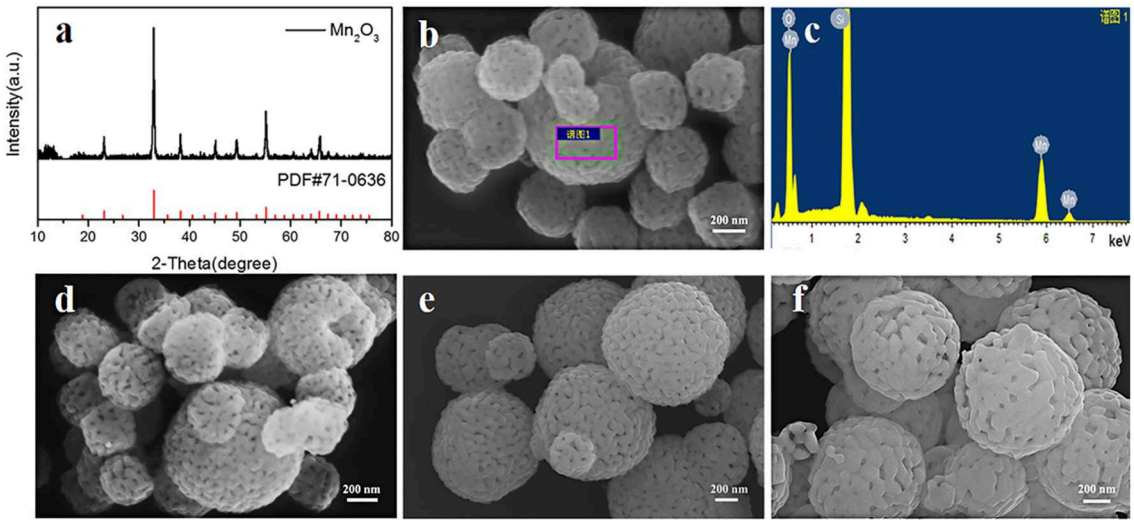


**FIGURE 7 | (a)** XRD pattern of $Mn_2O_3$ heated at 600°C for 5 h, **(b,c)** SEM image and EDS result of $Mn_2O_3$ heated at 600°C for 5 h, **(d–f)** SEM images of $Mn_2O_3$ heated at different temperature and time, **(d)** 600°C, 10 h **(e)** 600°C, 20 h **(f)** 700°C, 10 h.

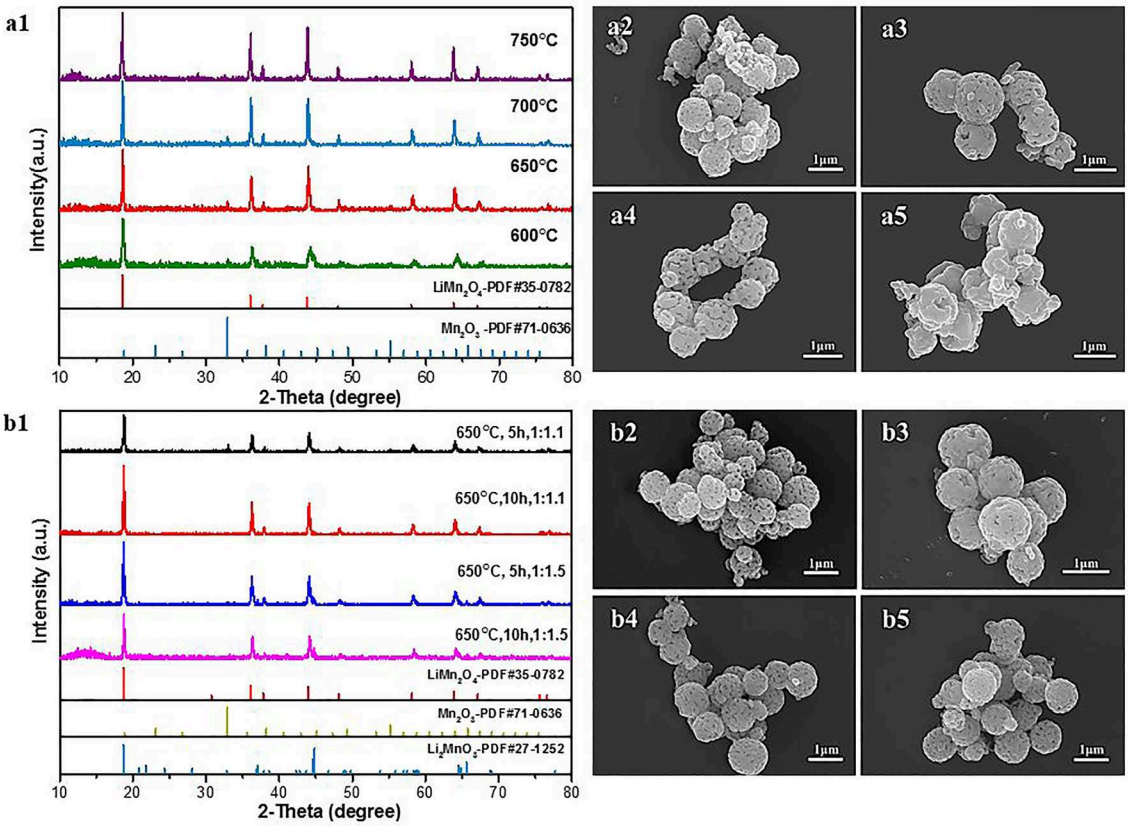


**FIGURE 8 | (a1)** XRD patterns of $LiMn_2O_4$ heated at different temperature. **(a2–a5)** SEM images of $LiMn_2O_4$ heated at different temperature for 5 h. **(a2)** 600°C **(a3)** 650°C **(a4)** 700°C **(a5)** 750°C. **(b1)** XRD patterns of $LiMn_2O_4$ heated at different $Mn_2O_3$: LiOH and calcination times. **(b2–b5)** SEM images of $LiMn_2O_4$ heated at different $Mn_2O_3$:LiOH and calcination times. **(b2)** 1:1.1, 5 h **(b3)** 1:1.1, 10 h **(b4)** 1:1.5, 5 h **(b5)** 1:1.5, 10 h.

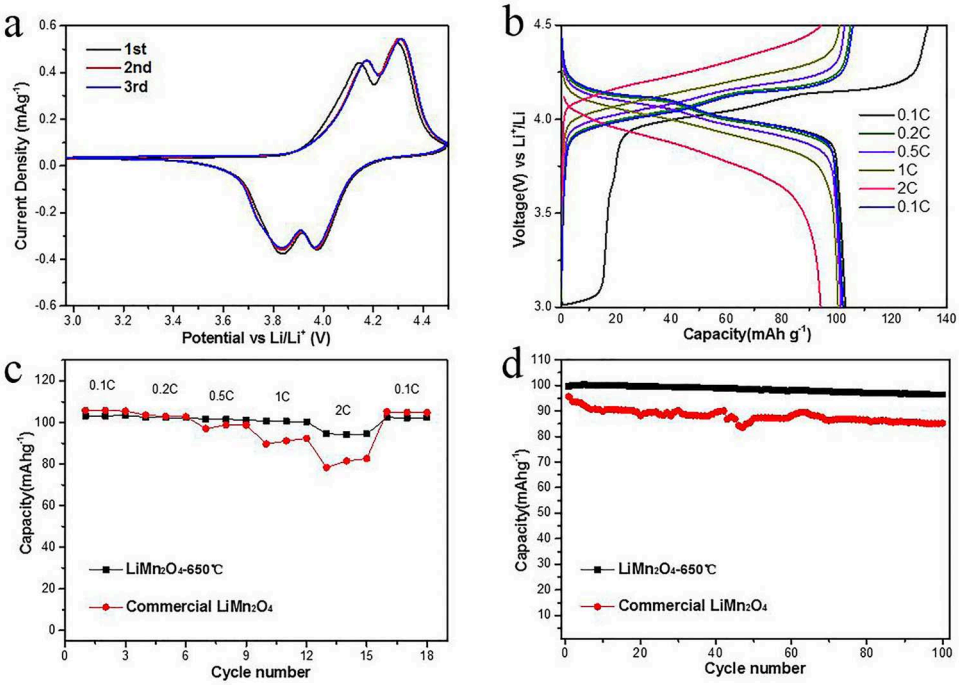


**FIGURE 9 |** Electrochemical performances of the synthetic porous $LiMn_2O_4$ spheres. **(a)** CV curves at a scan rate of 0.1 mV $s^{-1}$ in the voltage range of 3.0–4.5 V (vs. $Li/Li^+$); **(b)** discharge-charge curves at different rate from 0.1 to 2.0 C **(c)** variation of discharge capacity vs. cycle number of synthetic porous $LiMn_2O_4$ electrodes at 0.1–2.0 C rate; **(d)** cycle performance of synthetic porous $LiMn_2O_4$ at 1.0 C rate.

$LiMn_2O_4$ is shown in **Figure 9a**. Two pairs of separate redox peaks were observed form the CV curves of the synthesized sample, which correspond to the two-step insertion/deinsertion of lithium ion (Thackeray et al., 1983). **Figure 9b** reveals the current charge/discharge measurement by different rates over a voltage range of 3.0–4.5 V. The discharge capacities at rates of 0.1, 0.2, 0.5, 1.0, and 2.0 C were 103.18, 102.33, 101.50, 100.51, and 94.23 mAh $g^{-1}$, respectively. The rate performance is shown in **Figure 9c**. As can be seen, the rate performance of $LiMn_2O_4$ synthesized at 650°C is quite good, which demonstrates clearly slower capacity decay with increasing discharge rates. For example, the porous $LiMn_2O_4$ microspheres retain a capacity of 94.23 mAh $g^{-1}$, which is 91.3% of the initial capacity at rate of 0.1 C. This is much higher than that (76%) of the commercial $LiMn_2O_4$ powders at the same rate. When the current went back to a rate of 0.1 C, a capacity of 102.27 mAh $g^{-1}$ was resumed. The cycle stability of $LiMn_2O_4$ synthesized at 650°C at 1.0 C is shown in **Figure 9d**. The capacity of synthesized $LiMn_2O_4$ remains at 96.42 mAh $g^{-1}$ after 100 cycles and drops by only 3.24% compared to that of the first cycle. For comparison, the commercial $LiMn_2O_4$ exhibits a discharge capacity of 85.15 mAh $g^{-1}$ after 100 cycles, which is much lower than that of the synthesized porous $LiMn_2O_4$ microspheres sample. The good rate and cycling performance of the samples prepared are ascribed to a well-defined structure such as uniform size and high porosity, which is effective in increasing contact area, shortening the transport distance of lithium ions and enhancing the structural stability of electrode material.

## CONCLUSION

In summary, porous $LiMn_2O_4$ microspheres with an average diameter of about 1 μm have been successfully synthesized by using molten LiOH and porous $Mn_2O_3$ spheres as templates. The morphology and particle size of the products could be conveniently controlled by changing the reactant ratio, pH, adding mode, heating time, etc. The morphology of $MnCO_3$ was crucial for the preparation of porous $LiMn_2O_4$ microspheres and was mainly affected by the concentration of reactants and pH value of the solution during the chemical precipitation process. The optimum concentrations of $MnSO_4$ and $NH_4HCO_3$ were 0.036 and 0.36 M, respectively, with appropriate pH of 7.5. During the lithiation of $Mn_2O_3$ microspheres, the heating temperature and the ratio between $Mn_2O_3$ and lithium salt were the most significant variables in terms of control over the morphology and purity of the $LiMn_2O_4$ microspheres. Excessive or low temperature would cause the collapse or agglomeration of the prepared $LiMn_2O_4$ microspheres. In addition, unreacted $Mn_2O_3$ can be found in the final products when the amount of lithium salt was deficient. Instead, the byproduct of $Li_2MnO_3$ was easy to generate when there was too much lithium salt. Our work suggested that the uniform porous $LiMn_2O_4$ microspheres were synthesized with the optimum molar ratio of $Mn_2O_3$:LiOH

= 1: 1.1 and heated at 650°C for 10 h. Compared with the commercial $LiMn_2O_4$ powder, the synthesized $LiMn_2O_4$ microspheres present better rate capability and cyclability. This work can provide some guidance for the design and synthesis of porous $LiMn_2O_4$ microspheres or other LIBs' electrode materials.

## DATA AVAILABILITY

The raw data supporting the conclusions of this manuscript will be made available by the authors, without undue reservation, to any qualified researcher. Requests to access the datasets should be directed to liuhao1398@cugb.edu.cn.

## AUTHOR CONTRIBUTIONS

YH and ZZ carried out the experiment and wrote the manuscript. PF and YW participated in the experiment. GL and LM contributed to the discussion. HL and LL supervised the experiment and proofread the manuscript.

## FUNDING

This work is supported by the National Natural Science Foundation of China (No. 21875223) and the Fundamental Research Funds for the Central Universities (No. 649911023).

## REFERENCES

Aurbach, D., Levi, M. D., Gamulski, K., Markovsky, B., Salitra, G., Levi, E., et al. (1999). Capacity fading of $Li_xMn_2O_4$ spinel electrodes studied by XRD and electroanalytical techniques. *J. Power Sources* 81–82, 472–479. doi: 10.1016/S0378-7753(99)00204-9

Biernacki, L., and Pokrzywnicki, S. (1999). The thermal decomposition of manganese carbonate thermogravimetry and exoemission of electrons. *J. Therm. Anal. Calorim.* 55, 227–232. doi: 10.1023/A:1010165029080

Chen, D., Lou, Z., Jiang, K., and Shen, G. (2018). Device configurations and future prospects of flexible/stretchable lithium-ion batteries. *Adv. Funct. Mater.* 28:1805596. doi: 10.1002/adfm.201805596

Chen, H., Zhang, B., Zhang, J., Yu, W., Zheng, J., Ding, Z., et al. (2018). *In-situ* grown $SnS_2$ nanosheets on rGO as an advanced anode material for lithium and sodium ion batteries. *Front. Chem.* 6:629. doi: 10.3389/fchem.2018.00629

Etacheri, V., Marom, R., Elazari, R., Salitra, G., and Aurbach, D. (2011). Challenges in the development of advanced li-ion batteries: a review. *Energ. Environ. Sci.* 4:3243. doi: 10.1039/c1ee01598b

Guo, D., Chang, Z., Tang, H., Li, B., Xu, X., Yuan, X.-Z., et al. (2014). Electrochemical performance of solid sphere spinel $LiMn_2O_4$ with high tap density synthesized by porous spherical $Mn_3O_4$. *Electrochim. Acta* 123, 254–259. doi: 10.1016/j.electacta.2014.01.030

He, X., Li, J., Cai, Y., Jiang, C., and Wan, C. (2006). Preparation of spherical spinel $LiMn_2O_4$ cathode material for Li-Ion batteries. *Mater. Chem. Phys.* 95, 105–108. doi: 10.1016/j.matchemphys.2005.06.006

Hong, Y., Legge, R. L., Zhang, S., and Chen, P. (2003). Effect of amino acid sequence and ph on nanofiber formation of self-assembling peptides EAK16-II and EAK16-IV. *Biomacromolecules* 4, 1433–1442. doi: 10.1021/bm0341374

Hussain, A., Filiatrault, M., and Guiot, S. R. (2017). Acidogenic digestion of food waste in a thermophilic leach bed reactor: effect of pH and leachate recirculation rate on hydrolysis and volatile fatty acid production. *Bioresour. Technol.* 245, 1–9. doi: 10.1016/j.biortech.2017.08.130

Iqbal, A., Iqbal, Y., Chang, L., Ahmed, S., Tang, Z., and Gao, Y. (2012). Enhanced electrochemical performance of La- and Zn-Co-doped $LiMn_2O_4$ spinel as the cathode material for lithium-ion batteries. *J. Nanopart. Res.* 14:1206. doi: 10.1007/s11051-012-1206-9

Jeong, M., Lee, M.-J., Cho, J., and Lee, S. (2015). Surface Mn oxidation state controlled spinel $LiMn_2O_4$ as a cathode material for high-energy Li-Ion batteries. *Adv. Energy Mater.* 5:1500440. doi: 10.1002/aenm.201500440

Kloprogge, J. T., Hickey, L., and Frost, R. L. (2004). The effects of synthesis pH and hydrothermal treatment on the formation of zinc aluminum hydrotalcites. *J. Solid State Chem.* 177, 4047–4057. doi: 10.1016/j.jssc.2004.07.010

Kong, P. S., Pérès, Y., Wan Daud, W. M. A., Cognet, P., and Aroua, M. K. (2019). Esterification of glycerol with oleic acid over hydrophobic zirconia-silica acid catalyst and commercial acid catalyst: optimization and influence of catalyst acidity. *Front. Chem.* 7:205. doi: 10.3389/fchem.2019.00205

Lai, F., Zhang, X., Wang, H., Hu, S., Wu, X., Wu, Q., et al. (2016). Three-dimension hierarchical $Al_2O_3$ nanosheets wrapped $LiMn_2O_4$ with enhanced cycling stability as cathode material for lithium ion batteries. *ACS Appl. Mater. Inter.* 8, 21656–21665. doi: 10.1021/acsami.6b05640

Lee, H.-W., Muralidharan, P., Ruffo, R., Mari, C. M., Cui, Y., and Kim, D. K. (2010). Ultrathin spinel $LiMn_2O_4$ nanowires as high power cathode materials for Li-Ion batteries. *Nano Lett.* 10, 3852–3856. doi: 10.1021/nl101047f

Levi, E., Levi, M. D., Salitra, G., Aurbach, D., Oesten, R., Heider, U., et al. (1999). *In situ* XRD study of Li deintercalation from two different types of $LiMn_2O_4$ spinel. *Solid State Ionics* 126, 109–119. doi: 10.1016/S0167-2738(99)00219-2

Lipu, M. S. H., Hannan, M. A., Hussain, A., Hoque, M. M., Ker, P. J., Saad, M. H. M., et al. (2018). A review of state of health and remaining useful life estimation methods for lithium-ion battery in electric vehicles: challenges and recommendations. *J. Clean. Prod.* 205, 115–133. doi: 10.1016/j.jclepro.2018.09.065

Liu, H., Zhou, Y., and Song, W. (2018). Facile synthesis of porous $LiMn_2O_4$ micro-/nano-hollow spheres with extremely excellent cycle stability as cathode of lithium-ion batteries. *J. Solid State Electr.* 22, 2617–2622. doi: 10.1007/s10008-018-3937-8

Lu, L., Han, X., Li, J., Hua, J., and Ouyang, M. (2013). A review on the key issues for lithium-ion battery management in electric vehicles. *J. Power Sources* 226, 272–288. doi: 10.1016/j.jpowsour.2012.10.060

Nagao, D., Osuzu, H., Yamada, A., Mine, E., Kobayashi, Y., and Konno, M. (2004). Particle formation in the hydrolysis of tetraethyl orthosilicate in pH buffer solution. *J. Colloid Interf. Sci.* 279, 143–149. doi: 10.1016/j.jcis.2004.06.041

Park, Y., Jun, S., Kim, S., and Lee, D.-H. (2010). Design optimization of a loop heat pipe to cool a lithium ion battery onboard a military aircraft. *J. Mech. Sci. Technol.* 24, 609–618. doi: 10.1007/s12206-009-1214-6

Qian, J., Zhou, M., Cao, Y., Ai, X., and Yang, H. (2010). Template-free hydrothermal synthesis of nanoembossed mesoporous $LiFePO_4$ microspheres for high-performance lithium-ion batteries. *J. Phys. Chem. C* 114, 3477–3482. doi: 10.1021/jp912102k

Qu, Q., Fu, L., Zhan, X., Samuelis, D., Maier, J., Li, L., et al. (2011). Porous $LiMn_2O_4$ as cathode material with high power and excellent cycling for aqueous rechargeable lithium batteries. *Energ. Environ. Sci.* 4, 3985–3990. doi: 10.1039/C0EE00673D

Ren, L., Teng, C., Zhu, L., He, J., Wang, Y., Zuo, X., et al. (2014). Preparation of uniform magnetic recoverable catalyst microspheres with hierarchically mesoporous structure by using porous polymer microsphere template. *Nanoscale Res. Lett.* 9:163. doi: 10.1186/1556-276X-9-163

Simon, F., Szab,ó, M., and Fábián, I. (2019). pH controlled byproduct formation in aqueous decomposition of N-Chloro- α-Alanine. *J. Hazard. Mater.* 362, 286–293. doi: 10.1016/j.jhazmat.2018.09.004

Smart, M. C., Ratnakumar, B. V., Whitcanack, L. D., Chin, K. B., Surampudi, S., Gitzendanner, R., et al. (2004). Lithium-ion batteries for aerospace. *IEEE Aero. El Sys. Mag.* 19, 18–25. doi: 10.1109/MAES.2004.1263988

Tang, M., Yuan, A., Zhao, H., and Xu, J. (2013). High-performance $LiMn_2O_4$ with enwrapped segmented carbon nanotubes as cathode material for energy storage. *J. Power Sources* 235, 5–13. doi: 10.1016/j.jpowsour.2013.01.182

Tang, W., Wang, X. J., Hou, Y. Y., Li, L. L., Sun, H., Zhu, Y. S., et al. (2012). Nano $LiMn_2O_4$ as cathode material of high rate capability for lithium ion batteries. *J. Power Sources* 198, 308–311. doi: 10.1016/j.jpowsour.2011.09.106

Thackeray, M. M., David, W. I. F., Bruce, P. G., and Goodenough, J. B. (1983). Lithium insertion into manganese spinels. *Mater. Res. Bull.* 18, 461–472. doi: 10.1016/0025-5408(83)90138-1

Wakihara, M. (2001). Recent developments in lithium ion batteries. *Mat. Sci. Eng. R* 33, 109–134. doi: 10.1016/S0927-796X(01)00030-4

Wang, P. B., Luo, M. Z., Zheng, J. C., He, Z. J., Tong, H., and Yu, W. J. (2018). Comparative investigation of $0.5Li_2MnO_3{\cdot}0.5LiNi_{0.5}Co_{0.2}Mn_{0.3}O_2$ cathode materials synthesized by using different lithium sources. *Front. Chem.* 6:159. doi: 10.3389/fchem.2018.00159

Wang, Y., Shao, X., Xu, H., Xie, M., Deng, S., Wang, H., et al. (2013). Facile synthesis of porous $LiMn_2O_4$ spheres as cathode materials for high-power lithium ion batteries. *J. Power Sources* 226, 140–148. doi: 10.1016/j.jpowsour.2012.10.077

Xu, H., Chen, Y., Li, Y., Kong, L., Li, H., Xu, C., et al. (2018). Synthesis of single-crystal magnesium-doped spinel lithium manganate and its applications for lithium-ion batteries. *J. Solid State Electr.* 22, 3735–3742. doi: 10.1007/s10008-018-4072-2

Yin, H., Zhao, Y., Hua, Q., Zhang, J., Zhang, Y., Xu, X., et al. (2019). Controlled synthesis of hollow $\alpha$-$Fe_2O_3$ microspheres assembled with ionic liquid for enhanced visible-light photocatalytic activity. *Front. Chem.* 7:58. doi: 10.3389/fchem.2019.00058

Zhu, Q., Zheng, S., Lu, X., Wan, Y., Chen, Q., Yang, J., et al. (2016). Improved cycle performance of $LiMn_2O_4$ cathode material for aqueous rechargeable lithium battery by $LaF_3$ coating. *J. Alloy. Compd.* 654, 384–391. doi: 10.1016/j.jallcom.2015.09.085

**Conflict of Interest Statement:** The authors declare that the research was conducted in the absence of any commercial or financial relationships that could be construed as a potential conflict of interest.